Proceedings of the IASS Annual Symposium 2025
"The living past as a source of innovation"
27 October–31 October 2025, México City, México>
<Juan Gerardo Oliva, Juan Ignacio del Cueto, Elisa Drago (eds.)

Selfstressed Tensegrity-Origami Structures with Programmed Geometrically Nonlinear Response

Andrea MICHELETTI* a, Claudio INTRIGILAb, Filipe A. dos SANTOS c, Simon D. GUEST d, Alessandro TIERO a

*, a Dipartimento di Ingegneria Civile e Ingegneria Informatica, University of Rome Tor Vergata Via Politecnico 1, 00133, Rome, Italy Email micheletti@ing.uniroma2.it

^b Dipartimento di Ingegneria dell'Impresa 'Mario Lucertini', University of Rome Tor Vergata, Rome, Italy ^c Civil Engineering Dept., Facultade de Ciências e Tecnologia, Universidade NOVA de Lisboa, Caparica, Portugal ^d Department of Engineering, University of Cambridge, Cambridge, UK

Abstract

Origami structures have been extensively studied in the literature to design transformable systems with diverse mechanical properties. Recent research has demonstrated that certain origami structures exhibit bistable behavior, which can be leveraged for the development of modular multistable systems. In this study, we explore the connection between certain tensegrities and the origami structures of corresponding geometry to establish a systematic approach for designing prestressed origami structures with tailored nonlinear responses, such as stiffening, softening, and bistability. The procedure is illustrated by the case of the Kresling origami, which corresponds to the classical tensegrity frustum. First, a geometric analytical condition is derived to show that the Kresling origami can be given a geometric frustration leading to a selfstressed state related to the one in the tensegrity frustum. Then numerical simulations are conducted to evaluate the static response in both the prestressed and the bistable regimes. The results illustrate that tensegrity-inspired geometric design enables the realization of origami structures with controlled nonlinear response to external loads. By integrating this design methodology with existing tensegrity form-finding techniques, our approach facilitates the discovery of novel origami structures with programmable nonlinear behaviors, expanding the potential of multistable metamaterials and adaptive structural systems.

Keywords: tensegrity structures, origami structures, selfstressed structures, conceptual design, morphology, formfinding, multistability, nonlinear metamaterials

1. Introduction

Mechanical metamaterials offer novel capabilities by exploiting carefully designed geometric architectures rather than the mechanical properties of the constituent material. Among these, tensegrity-inspired and origami-based structures can enable a programmable mechanical response, multistability, and shape reconfiguration. These characteristics are essential in fields ranging from deployable systems and aerospace to soft robotics and mechanical computing [1, 2].

Tensegrity-like metamaterials utilize the properties inherited from the parent tensegrity structures to achieve controllable non-linear behaviors. Vangelatos *et al.* fabricated nanoscale tensegrity-like lattices based on tensegrity frustums through multiphoton lithography, achieving programmable snapping responses under axial compression [3]. Recent advancements by Intrigila *et al.* demonstrated bistable tensegrity-like frustums produced via additive manufacturing of monolithic compliant elements, thus removing the need for cable-strut assemblies [4]. This concept was subsequently extended to multistable

tensegrity-inspired chains [5] (Figure 1). These advances affirm the feasibility of modular tensegrity-like systems across multiple scales.

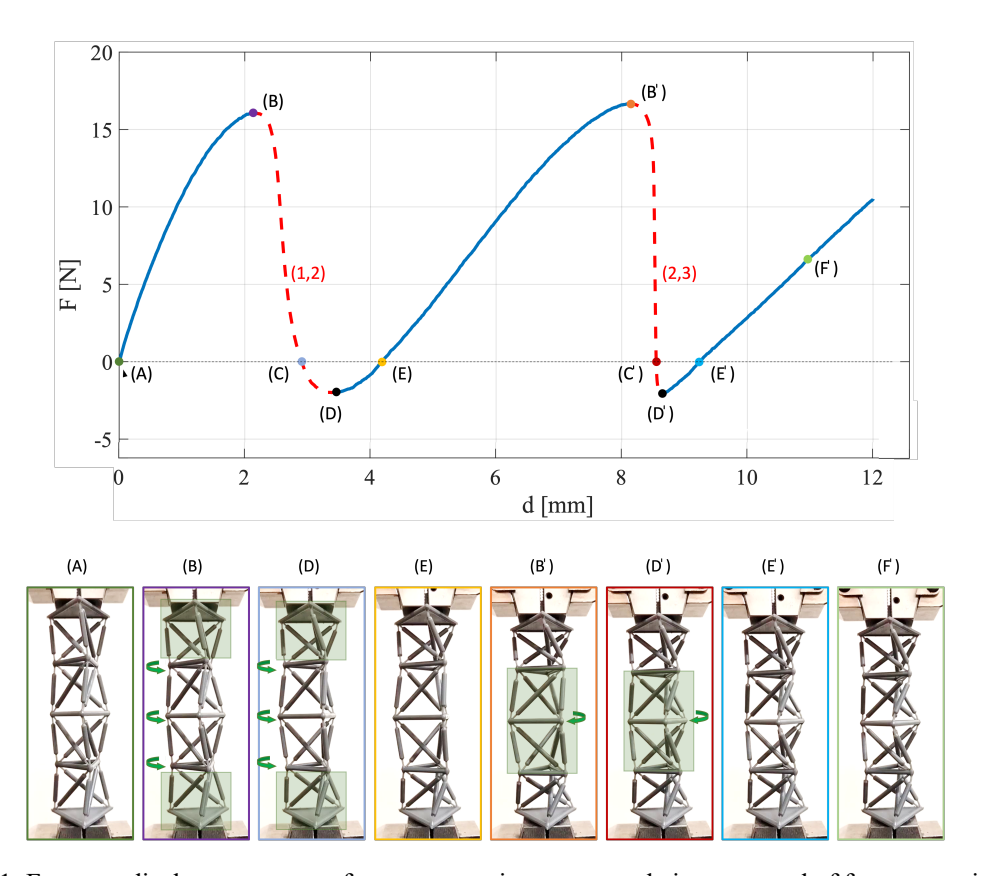


Figure 1: Force-vs-displacement curve for a compression test on a chain composed of four tensegrity-like frustums with alternating handedness (redrawn from Intrigila *et al.* [5]).

Analogously, Kresling origami structures exploit buckling-induced multistability and intrinsic axial-torsional coupling (Figures 2 and 3). Melançon *et al.* leveraged multistability in inflatable origami structures to achieve multimodal deformation from a single pressure input [6]. Studies by Novelino *et al.* introduced untethered magnetic actuation for Kresling microrobots [7], while Paulino *et al.* proposed programmable stiffness in modular origami chains [8]. Other works by Kidambi and Wang and by Kaufmann *et al.* explored dynamic deployment and soft robotics applications using reconfigurable Kresling-based mechanisms [9, 10]. Enhanced fabrication techniques, such as multimaterial 3D printing of Kresling units, were proposed by Khazaaleh *et al.*, [11].

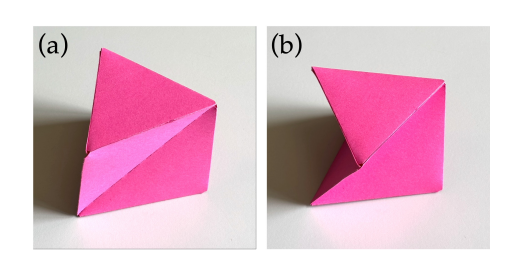


Figure 2: A Kresling origami unit in its two stable configurations.

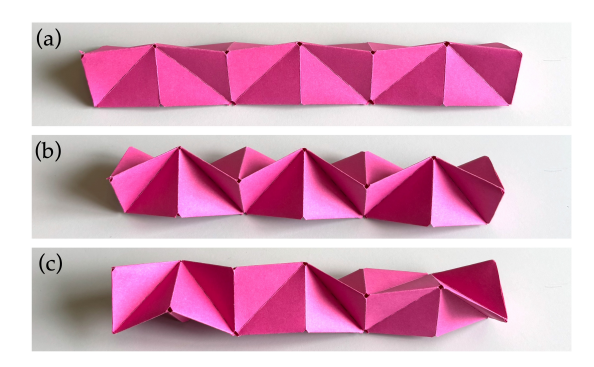


Figure 3: Three different stable configurations of a Kresling origami composed of six units with alternating handedness.

Despite significant progress, the connection between tensegrity frustums and Kresling origami is not well recognized in the literature, although it was already mentioned in the work by Intrigila *et al.* [5]. In this study, we first explore this connection in detail. We describe prestressed Kresling origami, in which geometric frustration leads to a selfstressed state related to the one in the classical tensegrity frustum. A new geometric analytical condition is derived to guide the design of both bistable and prestressed Kresling origami. We then present the results of several numerical compression tests carried out using a literature reduced-order model. These results illustrate various types of mechanical responses featured by tensegrity-like and Kresling origami frustums that can be programmed by selecting their geometry.

2. Geometry and selfstress state of the Kresling origami and the tensegrity frustum

A right tensegrity frustum with n bars can be obtained from a corresponding right frustum with regular n—gonal base by placing cables on the edges, noncontiguous struts along the diagonal of the side faces, and by rotating the top base with respect to the bottom base by a certain angle about the frustum axis, considered vertical. Figure 4(a) shows an instance of tensegrity frustum with triangular base (n = 3).

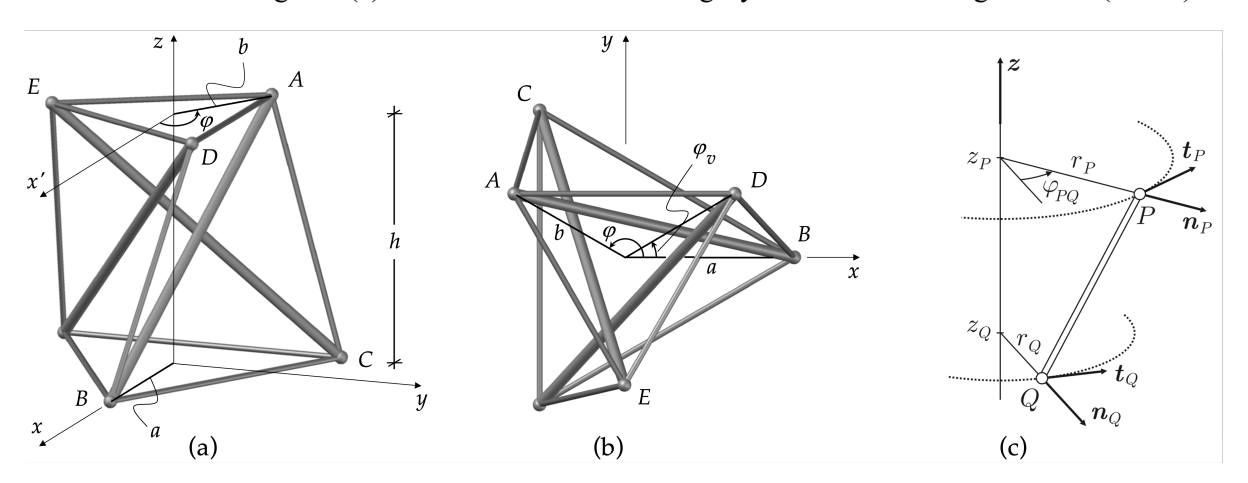


Figure 4: (a) A tensegrity frustum with triangular base (n = 3) and the geometric parameters determining its configuration. (b) Top view. (c) Local frames for a member PQ in cylindrical coordinates.

Analogously, the Kresling origami in Figure 1 can be obtained by placing triangular panels in correspondence to the triangles of edges of the tensegrity frustum in Figure 4(a). In the following, we indicate the edges of the Kresling origami using the terms *cable* and *strut* with reference to the corresponding edges of the tensegrity frustum. The geometric parameters identifying a tensegrity or Kresling origami frustum can be chosen as follows (Figure 4(a)): the twist angle, φ , that determines the relative rotation between the bases, counted from the position in which the struts lie in vertical planes

that contain the axis; the distance between bases, h; the circumscribed radii of the bottom and top bases, a and b, respectively.

It is well known that tensegrity frustums in stable equilibrium are found for values of the twist angle given by the form-finding relation $\varphi = \frac{\pi}{n} + \frac{\pi}{2}$, which is obtained by determining the selfstress solutions of the equilibrium equations of the corresponding bar framework. We now review the derivation of this relation to introduce a new related geometric compatibility condition.

On introducing the force coefficient of edge PQ as $q_{PQ} = \frac{t_{PQ}}{l_{PQ}}$, with t_{PQ} and l_{PQ} the axial force and the length of the edge, respectively, the equilibrium equation of node P be written as

$$\sum_{O} q_{PO}(\boldsymbol{p}_{P} - \boldsymbol{p}_{O}) = \boldsymbol{f}_{P} , \qquad (1)$$

with the summation extended to every node Q that is connected to node P. The relative position of node P with respect to node Q is written in the local reference frame $\{P; n_P, t_P, z\}$, for the radial, circumferential and vertical directions, respectively, associated with the cylindrical coordinate system centered on the cyclic-symmetry axis of the frustum (see Figure 4(c)):

$$\boldsymbol{p}_{P} - \boldsymbol{p}_{Q} = (r_{P} - r_{Q}\cos\varphi_{PQ})\boldsymbol{n}_{P} + r_{Q}\sin\varphi_{PQ}\boldsymbol{t}_{P} + (z_{P} - z_{Q})\boldsymbol{z}. \tag{2}$$

With reference to Figure 4 (a, b), the equilibrium equation of node A is

$$q_{AB}(\boldsymbol{p}_A - \boldsymbol{p}_B) + q_{AC}(\boldsymbol{p}_A - \boldsymbol{p}_C) + q_{AD}(\boldsymbol{p}_A - \boldsymbol{p}_D) + q_{AE}(\boldsymbol{p}_A - \boldsymbol{p}_E) = \mathbf{0}. \tag{3}$$

With the symmetry assumption $q_{AD} = q_{AE}$, and by using (2), the equilibrium equation (3) can be written in matrix form as

$$\begin{pmatrix} b - a\cos\varphi & b - a\cos\left(\varphi - \frac{2\pi}{n}\right) & 2b(1 - \cos\frac{2\pi}{n}) \\ a\sin\varphi & a\sin\left(\varphi - \frac{2\pi}{n}\right) & 0 \\ h & h & 0 \end{pmatrix} \begin{pmatrix} q_{AB} \\ q_{AC} \\ q_{AD} \end{pmatrix} = (\mathbf{0}), \quad (4)$$

where we considered that $\varphi_{AB} = \varphi$, $\varphi_{AC} = \varphi_{EB} = \varphi_v = \varphi - \frac{2\pi}{n}$, $\varphi_{AD} = \frac{2\pi}{n} = -\varphi_{AE}$ (see Figure 4 (b)). To have non-null solutions, the determinant of the coefficient matrix must be equal to zero, a condition that leads to

$$0 = \sin \varphi - \sin \varphi_v = \sin \varphi - \sin \left(\varphi - \frac{2\pi}{n}\right) = 2\sin \frac{\pi}{n}\cos \left(\varphi - \frac{\pi}{n}\right). \tag{5}$$

Since $n \ge 3$, the meaningful solution of (5) are $\varphi = \frac{\pi}{n} + \frac{\pi}{2}$, and $\varphi = \frac{\pi}{n} - \frac{\pi}{2}$. By substituting the first solution into the equilibrium equation (4) using the angle-shift formulas, $\sin\left(\frac{\pi}{n} + \frac{\pi}{2}\right) = \cos\frac{\pi}{n}$, $\cos\left(\frac{\pi}{n} + \frac{\pi}{2}\right) = -\sin\frac{\pi}{n}$, we have

$$\begin{pmatrix} b + a\sin\frac{\pi}{n} & b - a\sin\frac{\pi}{n} & 2b\left(1 - \cos\frac{2\pi}{n}\right) \\ a\cos\frac{\pi}{n} & a\cos\frac{\pi}{n} & 0 \\ h & h & 0 \end{pmatrix} \begin{pmatrix} q_{AB} \\ q_{AC} \\ q_{AD} \end{pmatrix} = (\mathbf{0}), \tag{6}$$

therefore,

$$q_{AB} = -q_{AC} , (7)$$

and

$$-a\sin\frac{\pi}{n}q_{AC} + b\left(1 - \cos\frac{2\pi}{n}\right)q_{AD} = 0, \qquad (8)$$

that is.

$$q_{AC} = \frac{b}{a} \frac{1 - \cos\frac{2\pi}{n}}{\sin\frac{\pi}{n}} q_{AD} = 2\frac{b}{a} \sin\frac{\pi}{n} q_{AD} . \tag{9}$$

On denoting by the subscripts s, v, a, and b the quantities associated with the struts, side cables, bottom cables, and top cables, respectively, we have that

$$q_{AB} = \frac{t_s}{l_s}$$
, $q_{AC} = \frac{t_v}{l_p}$, $q_{AD} = \frac{t_b}{l_p}$, (10)

and the relations (7), (9) can be re-expressed as

$$t_s = -q_0 l_s$$
, $t_v = q_0 l_v$, $t_b = q_0 a$, $t_a = q_0 b$, (11)

where we considered that $l_a=2a\sin\left(\frac{\pi}{n}\right)$, $l_b=2b\sin\left(\frac{\pi}{n}\right)$, and we set $q_{AC}=q_0>0$, a reference force coefficient for side cables, while the last relation is obtained by exchanging the role of bottom and top cables. Relations (11) show that the edge lengths of a tensegrity frustum determine the ratios between axial forces in the selfstress state. It can be seen that by substituting the second solution, $\varphi=\frac{\pi}{n}-\frac{\pi}{2}$, into the equilibrium equation, the axial forces in the top and side cables have opposite signs and the selfstress state is not admissible. Thus, selfstressable configurations are obtained for a value of the twist angle equal to

$$\varphi_0 := \frac{\pi}{2} + \frac{\pi}{n},\tag{12}$$

while the other geometric parameters, h, a, and b, can be arbitrarily assigned.

We now derive a geometric compatibility condition that provide insight to the form finding of Kresling origami structures with specific features, such as bistability or prestressability. With reference to Figure 4(c), the squared length of the edge PQ is $l_{PQ}^2 = (z_P - z_Q)^2 + r_P^2 + r_q^2 - 2 r_P r_Q \cos \varphi_{PQ}$. Then, the edge lengths of the struts and side cables can be expressed as

$$l_s^2 = h^2 + a^2 + b^2 - 2ab\cos\varphi$$
, $l_v^2 = h^2 + a^2 + b^2 - 2ab\cos\varphi_v$.

By subtraction, we get $l_s^2 - l_v^2 = -2ab (\cos \varphi - \cos \varphi_v)$.

On introducing the overtwist angle $\theta \coloneqq \phi - \phi_0$, recalling that $\phi_v = \phi - \frac{2\pi}{n}$, and expressing the twist as $\phi = \phi_0 + \theta = \frac{\pi}{2} + \frac{\pi}{n} + \theta$, the previous relation can be rewritten as

$$l_s^2 - l_v^2 = 4ab \sin\left(\frac{\pi}{n}\right) \cos\theta , \qquad (13)$$

that is,

$$\frac{l_s^2 - l_v^2}{4ab\sin(\frac{\pi}{n})} = \cos\theta.$$

Since $\cos \theta \in [-1,1]$, we have that

$$|l_s^2 - l_v^2| \le 4ab \sin\left(\frac{\pi}{n}\right),\tag{14}$$

a relation that can be interpreted as a buildability condition for both the tensegrity and the Kresling origami frustum. If the edges lengths satisfy this condition, then it is possible to build the corresponding three-dimensional structure. If the edges lengths are chosen according to the relation

$$l_s^2 = l_v^2 + 4ab\sin\left(\frac{\pi}{n}\right) + \delta ab, \qquad (15)$$

with δ a small negative value, then we can solve (13) for the overtwist θ to find

$$\theta = \pm \arccos\left(\frac{l_s^2 - l_v^2}{4ab\sin(\frac{\pi}{n})}\right),\tag{16}$$

which means that for the same assignment of edge lengths two configurations with equal and opposite overtwists exist. Relations (14)-(16) can be exploited to design Kresling origami frustums and corresponding bar frameworks with bistable behavior. If instead $|l_s^2 - l_v^2| > 4ab \sin\left(\frac{\pi}{n}\right)$, then no threedimensional configuration with those edge lengths exists: if the structure is assembled by putting together its parts, be them cables and struts, in the case of a tensegrity frustum, or origami panels, in the case of a Kresling origami, then it will not be possible to realize all connections between them. It is worth noticing that the right-hand side in (14) can be expressed as a function of the top and bottom edge lengths, l_a and l_b . It is easy to see that (14) also implies that, starting from a non-admissible set of edge lengths, we can decrease the lengths of the struts or increase the lengths of the cables until condition (14) is met. This is the typical situation of prestressed tensegrity systems, in which cables (struts) have a prestressed length that is longer (shorter) than their length at rest. Condition (14) proves that the Kresling origami can be realized as a prestressed structure. In fact, by choosing the edges lengths according to the relation (15) but with δ a small positive value, it is possible to realize a Kresling origami with frustrated geometry. Figure 5 shows two instances of paper models with slight or more pronounced frustration, causing the deformation of the origami panels. Figure 6 shows a developed Kresling origami strip with edge lengths satisfying (15) with $\delta > 0$ and the mismatch observed when trying to realize the connection between the first and last panel.

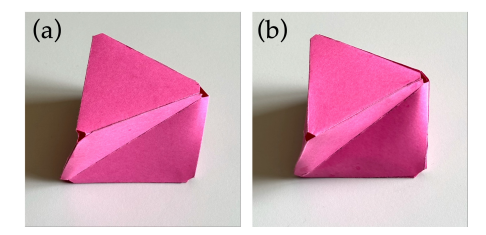


Figure 5: Two Kresling origami units with: (a) slight frustration and (b) pronounced frustration causing the warping of the origami panels.

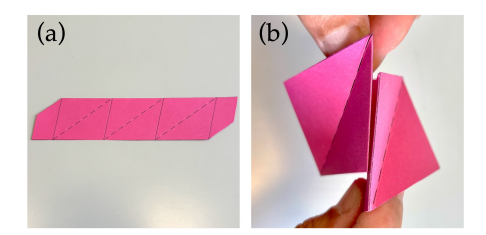


Figure 6: (a) A developed Kresling origami strip with edge lengths satisfying (15) when $\delta > 0$ and (b) the mismatch observed when trying to realize the connection between the first and last panel.

To understand the selfstress state of the Kresling origami, we consider for simplicity the case a = b, with $\theta = 0$ ($\varphi = \varphi_0$), and assume that internal actions between adjacent panels are exchanged at the vertices. The forces applied to the three vertices of the panel need to be coplanar to satisfy the equilibrium conditions. Figure 7 (a, b) shows the top and side view of one panel of the Kresling origami subjected to the internal forces at the vertices. The internal force at vertex B is decomposed along the directions parallel to the bottom cable BC and to the strut AB, and the internal force at C is decomposed along the directions parallel to the bottom cable BC and to the side cable AC. By symmetry considerations, the forces parallel to the strut and side cables at the vertices B and C are equal to those exchanged at vertex A by adjacent panels and denoted by $t_s/2$ and $t_v/2$, respectively, (Figure 7 (b)). The force components at B and C parallel to cable BC need to be equal and opposite for the resultant moment balance with pole A, and they are denoted by t_a . At vertex A, the two adjacent panels apply forces of same magnitude t_a along the directions parallel to AD and AE. The composition of these two forces results in the force $t_r = 2 t_a \sin\left(\frac{\pi}{n}\right)$ along the direction of the axis x'' (Figure 7 (a)). On considering that $\frac{t_r}{l_a} = \frac{t_a}{a}$, the equilibrium of the forces t_r , t_s , t_v acting on the panel is satisfied when $\frac{t_r}{l_a} = \frac{t_s}{l_s} = \frac{t_v}{l_v}$, that is, these force are directly proportional to the panel edge lengths. The composition of the forces at vertex A results in the force of magnitude $t_r/2 = t_a \sin\left(\frac{\pi}{n}\right)$ along the direction of the axis x'' (Figure 7(c)). The net forces at vertices A, B, and C of the panel are shown in Figure 7(d). These internal forces permit to give an interpretation of the deformation of the valley creases that is evident in Figure 5.

The frustrated Kresling origami and the tensegrity structure appear at first sight to carry the state of selfstress in very different ways: the Kresling has shear forces along edges, while the tensegrity has tension or compression in cables and struts. However, the following model makes the connection between these sets of forces clear. Consider if each panel in the Kresling only carries internal forces along its edges, as would happen if the middle of the panel had been removed. Then equilibrium of the forces applied to a single panel shows that the internal forces carried by the edges AB and AC of the panel have half the value of the force in the corresponding strut and cable in the tensegrity (cf Figure 7(e)), with the other half of the force carried in the panel on the other side of the hinge.

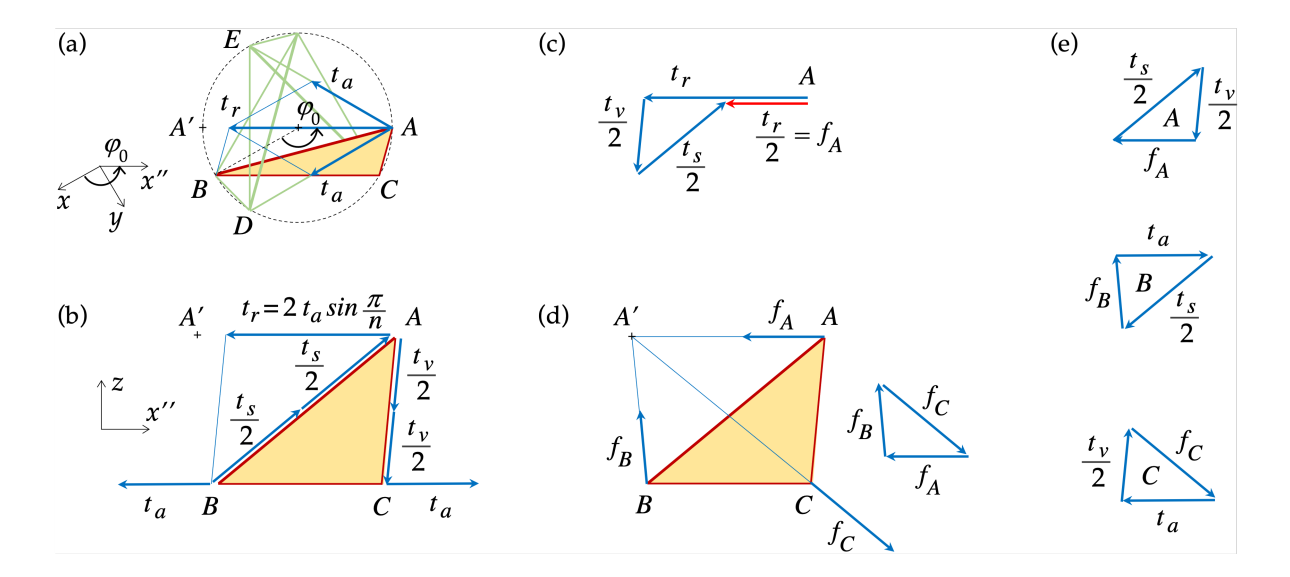


Figure 7: Representation of the selfstressing internal actions on an origami panel of a Kresling unit with a=b (detailed description in the main text). (a) Top view of the unit with a panel highlighted. (b) Side view of the highlighted panel. At vertex A, the two adjacent panels apply forces of same magnitude t_a along the directions parallel to AD and AE. The composition of these two forces results in the force t_r along the direction of the axis x''. The forces t_r , t_s , t_v are directly proportional to the panel edge lengths. (c) The composition of the forces at vertex A results in the force of magnitude $t_r/2$ along the direction of the axis x''. (d) Net forces f_A , f_B , f_C at vertices f_A , f_B , and f_B of the panel and the corresponding equilibrium triangle. (e) Equilibrium triangles at each vertex for the corresponding net force and the forces carried by the edges of the panel.

3. Programmable mechanical response

We have seen that the dimensionless parameter δ in (15) governs the response regimes of the tensegrity and Kresling origami frustums. The assembled structure is prestressed when $\delta > 0$, and it is stress-free when $\delta = 0$. In both these cases there is a single load-free equilibrium configuration with twist $\varphi = \varphi_0$ given by (12). When $\delta < 0$, the structure is bistable: there are two stress- and load-free equilibrium configurations with twist $\varphi = \varphi_0 + \theta$, and θ given by (16).

In this section we present the results of numerical simulations carried out with the use of a reduced-order stick-and-spring model [12] (see also [4]) that is analogous to the discrete models proposed in the literature [13,14,15]. Different Kresling units are tested under quasi-static compression. Strut and cable edges are modeled as axial springs, and a total of 2n rotational springs are added at selected junctions to capture the stiffness of the folds. Figure 8 shows the setup of the compression test and the location of the rotational springs on the Kresling unit. The axial and rotational springs have stiffness constant k_a and $k_r = \alpha k_a a b$, respectively, with α a tuning parameter. Prestress is introduced by assigning the prestrain $\epsilon_v = \frac{l_{vo} - l_v}{l_v}$ of the side cable edges, with l_{vo} their prestressed length. Base nodes are constrained in the vertical direction. The compressive force f associated with an imposed vertical displacement Δh between the top and bottom base of the unit is obtained as the sum of constraint reactions at one base. Figure 9(a) shows the dimensionless force-vs-displacement curves of the tests performed on prestressed units. The parameters of the simulation are n = 3, n = 4, n = 6, n = 1, n = 6, n = 1, n = 1, and prestrain values n = 1

shows the results of the compression tests for the bistable case considering same n, a, b, h, k_a, α , no prestrain $(\varepsilon_v = 0)$, and overtwist values $\theta = 0, -2, -5, -10, -15$. As might be expected, higher overtwist values are associated with more marked bistable responses.

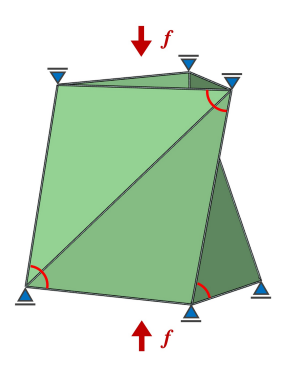


Figure 8: Compression test on a Kresling unit. Base nodes are constrained in the vertical direction. The red arcs show the position of the angular springs in the stick-and-spring model. A relative vertical displacement Δh is imposed between the top and bottom bases. The compressive force is computed as the sum of the constraint reactions at one base.

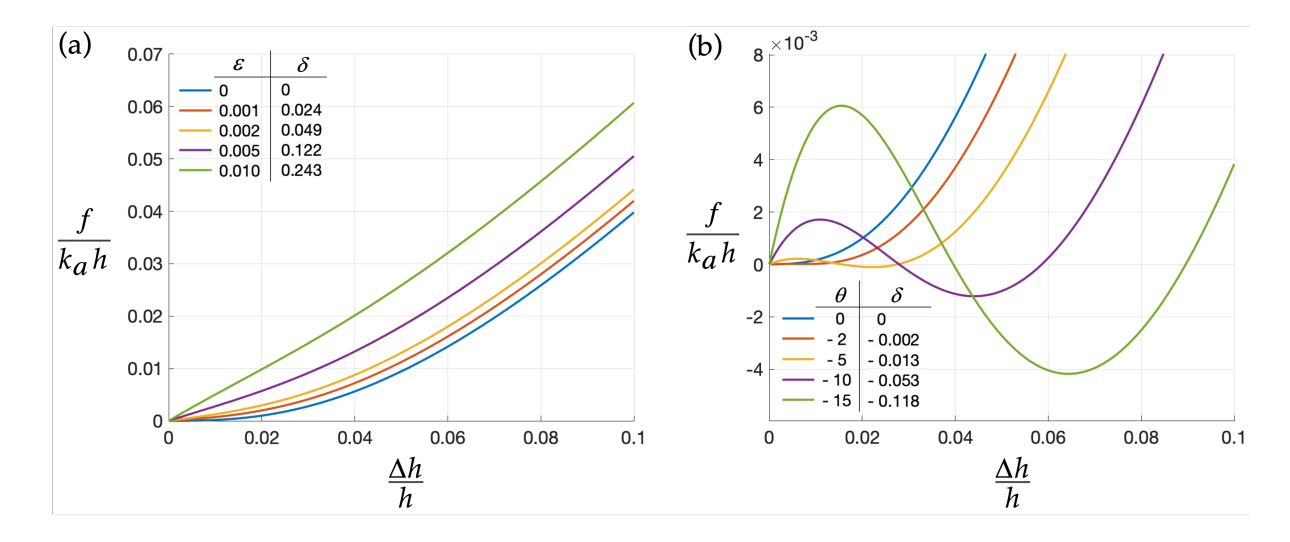


Figure 9: Different quasi-static responses of the Kresling unit under compression plotted as dimensionless force-vs-displacement curves: (a) increasing prestrain, $\varepsilon_v = 0,0.001,0.002,0.005,0.010$ ($\theta = 0$); (b) increasing overtwist, $\theta = 0, -2, -5, -10, -15$ ($\varepsilon_v = 0$). In all tests, n = 3, a = 4, b = 3, h = 6, $k_a = 1$, and $\alpha = 0.0002$. The corresponding values of the parameter δ governing the regime of the response are reported ($\delta > 0$, prestressed unit, $\delta < 0$, bistable unit).

5. Concluding remarks

In this work, we established a link between the tensegrity frustum and the Kresling origami. We showed that a Kresling origami unit can be realized as a selfstressed structure and that tensegrity-inspired geometric design enables Kresling units with tailored nonlinear mechanical responses. From a design perspective, the methodology introduced here can be extended to more complex geometries beyond the Kresling unit. Existing tensegrity geometries can be translated to origami configurations with programmable nonlinear response. Future research will focus on exploiting this concept for applications in energy dissipation, adaptive architecture, and deployable robotics.

Acknowledgements

This work was supported by University of Rome Tor Vergata, Italy through the project "Challeng: Challenging Education by Challenging Structures: Smart Interactive Didactical Tools for Engineers" within the "Ricerca Scientifica di Ateneo 2024" program.

References

- [1] A. Micheletti and P. Podio-Guidugli, "Seventy years of tensegrities (and counting)", *Archive of Applied Mechanics*, vol. 92, pp. 2525–2548, 2022.
- [2] D. Misseroni, P.P. Pratapa, K. Liu, B. Kresling, Y. Chen, C. Daraio and G.H. Paulino, "Origami engineering", *Nature Reviews Methods Primers*, vol. 40, p. 40, 2024.
- [3] Z. Vangelatos, A. Micheletti, C. P. Grigoropoulos and F. Fraternali, "Design and testing of bistable lattices with tensegrity architecture and nanoscale features fabricated by multiphoton lithography", *Nanomaterials*, vol. 10, no. 4, p. 652, 2020.
- [4] C. Intrigila, A. Micheletti, N.A. Nodargi, E. Artioli and P. Bisegna, "Fabrication and experimental characterisation of a bistable tensegrity-like unit for lattice metamaterials", *Additive Manufacturing*, vol. 57, p. 102946, 2022.
- [5] C. Intrigila, A. Micheletti, N.A. Nodargi and P. Bisegna, "Mechanical response of multistable tensegrity-like lattice chains", *Additive Manufacturing*, vol. 74, p. 103724, 2023.
- [6] D. Melançon, A. E. Forte, L. M. Kamp, B. Gorissen and K. Bertoldi, "Inflatable origami: multimodal deformation via multistability", *Advanced Functional Materials*, vol. 32, no. 35, p. 2201891, 2022.
- [7] L.S. Novelino, Q. Ze, S. Wu, G.H. Paulino, and R. Zhao, "Untethered control of functional origami microrobots with distributed actuation", *Proceedings of the National Academy of Sciences*, vol. 117, no. 39, pp. 24096-24101, 2020.
- [8] T. Zhao, X. Dang, K. Manos, Z. Shixi, J. Mandal, M. Chen and G.H. Paulino, "Modular chiral origami metamaterials", *Nature*, Vol. 640, pp. 931–940, 2025.
- [9] N. Kidambi, K.W. Wang, "Dynamics of kresling origami deployment", *Physical Reviews E*, Vol. 101, pp. 063003, 2020.
- [10] J. Kaufmann, P. Bhovad and S. Li, "Harnessing the multistability of Kresling origami for reconfigurable articulation in soft robotic arms", *Soft Robotics*, Vol. 9, No. 2, pp. 212-223, 2022.
- [11] S. Khazaaleh, R. Masana and M.F. Daqaq, "Combining advanced 3d printing technologies with origami principles: A new paradigm for the design of functional, durable, and scalable springs", *Composites B*, Vol. 236, pp. 109811, 2022.
- [12] A. Favata, A. Micheletti and P. Podio-Guidugli, "A nonlinear theory of prestressed elastic stick-and-spring structures", *International Journal of Engineering Science*, vol. 80, pp. 4–20, 2014.
- [13] M. Schenk and S.D. Guest, "Origami Folding: A Structural Engineering Approach", *Proceedings of the 5th International Conference on Origami in Science, Mathematics and Education and Folding Convention*, pp. 291–303, Singapore, 2010.
- [14] K. Liu and G.H. Paulino GH, "Nonlinear mechanics of non-rigid origami: an efficient computational approach", *Proceedings of the Royal Society A*, vol. 473, p. 20170348, 2017.
- [15] A. Ghassaei, E.D. Demaine and N. Gershenfeld, "Fast, interactive origami simulation using gpu computation", in *Proceedings of the 7th international meeting on origami in science, mathematics and education*, vol 4, pp. 1151–1166, Tarquin, Oxford, England, 2018.